Rate-Controlled Mercury Injection Experiments to Characterize Pore Space Geometry of Berea Sandstone

Walid Mohamed Mahmud[1,*]

[1]Department of Petroleum Engineering, Faculty of Engineering, University of Tripoli, Tripoli, Libya

Abstract. Interpretation of the relationship between heterogeneity and the flow in porous media is very important in increasing the recovery factor for an oil or gas reservoir. Capillarity for instance, controls fluids static distribution in a reservoir prior to production and remaining hydrocarbons after production commences. Therefore, capillary pressure data are used by petroleum engineers, geologists, and petrophysicists to evaluate production characteristics of petroleum accumulations. Conventional pressure-controlled mercury porosimetry produces an overall capillary pressure curve and pore throat size distribution data that provide little information about the porous medium structure and pore geometry. The present study provides information on three capillary pressure curves obtained from rate-controlled mercury injection porosimetry; one describes the larger pore spaces or pore bodies of a rock, another describes the smaller pores or pore throats that connect the larger pores, and a final curve which corresponds to the overall capillary pressure curve obtained from the conventional pressure-controlled mercury injection. An experimental constant-rate mercury injection apparatus was constructed that consists of a piston displacement pump, a computer controlled stepper motor drive and a core sample cell designed to minimize dead volume. The apparatus was placed in a glass chamber and subjected to an air bath to maintain a constant temperature of 27° C throughout the experiments. Then constant rate mercury injection experiments were performed on three Berea Sandstone core plugs. Results show that volume-controlled or rate-controlled porosimetry provides considerably more detailed data and information on heterogeneity and the statistical nature of pore space structure than the conventional pressure-controlled porosimetry as pressure fluctuations with time reveal menisci locations in pore bodies and pore throats. Moreover, pore size distributions based on volume-accessed pores and pore radii were obtained from the pressure versus saturation relationship.

1 Introduction

The main principle of capillary pressure measurements by mercury porosimetry is by the incremental increase of pressure while monitoring the increase in mercury saturation being injected into a porous core plug. Pressure-controlled porosimetry method, or the conventional technique, measures the capillary pressure curves in a way that it is possible to obtain one capillary pressure curve from different distributions of pore systems. Yuan and Swanson [1] introduced a pioneering method to Wood's metal porosimetry at which mercury was injected into a core plug at a very slow and constant flow rate. It was possible, through this method, to conceptually partition pore space into pore throats; which they named rison, pore bodies or subison besides the standard capillary pressure curve identical to that obtained from the pressure-controlled mercury porosimetry. Pressure-controlled mercury intrusion method may indirectly measure significantly narrow throats but does not detect larger pores that rate-controlled method detects as it quantitatively separates and characterizes throat and pore size distributions. Therefore, more accurate information can be obtained, from the rate-controlled method, about pore space characterization and micro-pore structure characteristic parameters. Moreover, rate-controlled mercury porosimetry yields information and data on the sizes and volumes of pore bodies or nodes and pore throats or links that can be utilized to calibrate network models that, in turn, used to estimate relative permeability, capillary pressure and residual saturation. Network models may also be used to validate correlated heterogeneity in rocks by comparing measured curves obtained from rate-controlled mercury injection and those predicted from network models.

Gao et al. [2] used rate-controlled or constant-rate mercury intrusion technique on tight core plugs to determine the size of pore and throat parameters. Zhang et al. [3] utilized rate-controlled mercury injection on tight sandstone core plugs to investigate pore-throat structure characteristics. Smith and Chatzis [4] developed a method of measuring the breakthrough capillary pressure involving a constant-rate injection technique. Zhang et al. [5] analyzed pore-throat structure effect of tight rocks on the seepage and storage capacity employing, among other techniques, rate-controlled mercury injection technique. Zhang et al. [6] performed constant-rate mercury injection experimental measurements in low permeability reservoirs to investigate poor correlation while calculating permeability. Wang et al. [7] recently studied the pore throat structure characteristics of sandy conglomerate and tight sandstone using constant-rate mercury injection along with the conventional constant-pressure mercury injection and micro CT scanning data. It was shown that substantial regions of the rock remain uninvaded at low and moderate non-wetting phase saturations [8]. However, the uninvaded regions then become filled as the non-wetting phase saturation increases indicating that correlated heterogeneity might exist at the core scale. Moreover, visual studies on sandstone pore casts showed correlations between pore body sizes and adjoining pore throats [9]. Therefore, it is important to consider and model spatial and local correlations in network models [10]. Mercury porosimetry was used to study the effect of pore-throat correlations; a widening drainage capillary pressure curves were noticed on correlated networks [11].

Rate-controlled and pressure controlled porosimetries and

* Corresponding author: w.mahmud@uot.edu.ly

scanning electron microscopy were utilized to study pore size distribution of bentonite [12]. The combined use of rate-controlled and pressure-controlled porosimetries was found the best for obtaining the bentonite full-scale pore size distribution while employing each method separately has its limitation.

Yao and Liu [13] compared between the conventional pressure-controlled mercury injection porosimetry, rate-controlled mercury injection porosimetry, micro focus computerized tomography and low-field nuclear magnetic resonance spectral analysis in measuring coals' pore size distribution. Pressure-controlled mercury injection method was found to have limitations such as coal sample destruction, due to high-pressure, and therefrom inaccurate estimations of coal pore size distribution, pore volume and porosity. Rate-controlled mercury injection method, on the other hand, was found effective and provided very detailed pore size distribution information of macropores but insufficient information on pore size distribution of mesopores.

Adams [14] incorporated nuclear magnetic resonance and conducted mercury injection capillary pressure measurements on carbonate and sandstone core plugs to determine large, medium, and small pore sizes, and their associated pore shapes. He calculated mercury injection capillary pressure curves and distributions of pore-throat aperture and compared the results with other techniques. It was possible to discriminate between pores of different genetic origin from one another by using a combination of pore size and pore geometry. Moreover, median pore-throat apertures were found strongly correlated to permeability.

In the present study, rate-controlled mercury porosimetry equipment was built and utilized to characterize pore morphologies by quantitatively dividing pore space into pore bodies and pore throats using Berea sandstone core plugs. Constant-rate mercury injection experiments yielded important structural parameters that includes throat and pore bodies volumes, pores radii distribution, independent pore bodies, throats and total capillary pressure curves. Pore bodies and throats might be orderly or disorderly distributed. Therefore, correlations might exist between the sizes and shapes of throats and pores over extended field-scale porous media or only over a few pores [15]. Data obtained may also be utilized in network modeling studies to identify the nature of spatial and pore throat and pore body correlations and heterogeneity in rocks.

2 Core plugs preparation and properties

Core plugs were sampled from a full diameter Berea sandstone core that has a gas permeability of 1.31 D. Core plugs were cylindrical in shape with similar dimensions and no visual irregular external surfaces. Porosity was measured separately for each core plug using helium gas expansion porosimeter based on the principle of Boyle's Law. A sealed reference chamber in the instrument is filled with helium gas at ambient temperature to a pressure of 100 psig. The core plug is then placed in another sealed chamber, connected to the reference chamber by a two-way valve. This valve when opened allows the gas in the reference chamber to expand into the combined volume of the two chambers. From Boyle's Law, the volume of the core plug chamber can be calculated when the volume of the reference chamber, the initial pressure and the final pressure are known. The porosity and the grain density were then calculated by determining the bulk volume, and the weight of the core plug. Pore volume of the core plug equals the bulk volume minus the grain volume. Porosity equals the core plug pore volume divided by the bulk volume. Distribution of core plugs porosities ranged from 28.2 to 30.7%. The permeability and porosity values indicate good reservoir rock quality.

3 Experimental equipment and methodology

The experimental equipment is shown schematically in Figure 1. Unlike the conventional mercury intrusion, quasi-static capillary equilibrium injection was achieved by injecting mercury at a very low and constant flow rate of 0.00000002 cc/sec. The experimental equipment consists of a stepper motor drive controlled by computer, a cell of 11 cc capacity to contain core plug designed to minimize dead volume, a piston displacement pump that is vertically mounted to eliminate air trapping. The cell is connected at the top through a vacuum port. Each core plug was preprocessed/placed under vacuum before mercury injection commences and the core plug becomes fully surrounded and submersed in mercury. Vacuum of fifty microns of mercury was applied for eight hours before conducting each experiment. A pressure transducer measures the pressure in the cell that is powered by a twelve-volt battery to minimize signal noise. Pressure transducer's range is from 0 to 100 psi with a resolution of +/- 0.00005 psi. The equipment was put in a glass built chamber, shown in Figure 2, at constant temperature of 27 °C. In order to maintain and control constant temperature throughout the experiments and to eliminate any possible thermal effects on pressure fluctuations, electric fan heater was placed inside the chamber that is visible in Figure 2. Volume measurement resolution was 0.000031 cc equivalent to one shaft encoder count. A program was generated to read the Hewlett Packard voltmeter and to control the stepper motor that drives the mercury injection pump. The outcome of the program is readings of the cumulative mercury injected volume, pressure and time. Pore volume invaded by mercury is then obtained from the cumulative pore volume filled by mercury and the overall pore volume of the core plug.

Figure 3 shows the overall, full scale, capillary pressure versus mercury pore volume injected saturation of the rate-controlled mercury injection experiments of the present work. Figures 4 and 5 show magnified sections of the data collected during the experiment; pore volume injected represents volume of mercury injected divided by ambient helium pore volume. Constant-rate mercury injection enables the division of the overall mercury injection capillary pressure curve into pores and throats mercury injection capillary pressure curves that are utilized to characterize throat and pore size distributions [1]. It is also possible analyzing throats and pores parameters including throats and pores radii distribution and the ratio between

them. Figure 5 shows the capillary pressure fluctuations and response corresponding to filling of interconnected pores. A sudden 'primary' drop in capillary pressure as mercury meniscus falls from a narrow pore throat into a wide pore body. Immediately afterwards, the capillary pressure gradually increases as mercury commences filling adjoining interconnected pore throats. This ensembles a drainage displacement at which non-wetting fluid, mercury in the present study, displaces wetting fluid, air, in the pore space of the rock. The instant pore-scale displacement events that occur are also referred to as Haines jumps [16].

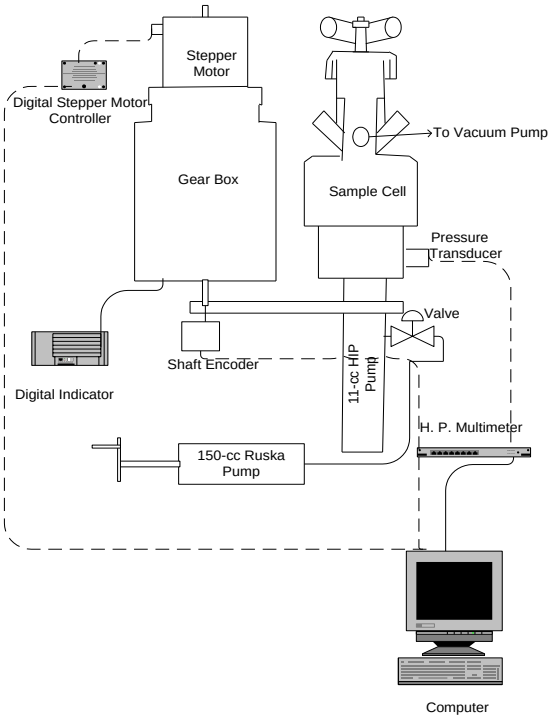

Figure 1: Schematic of experimental equipment.

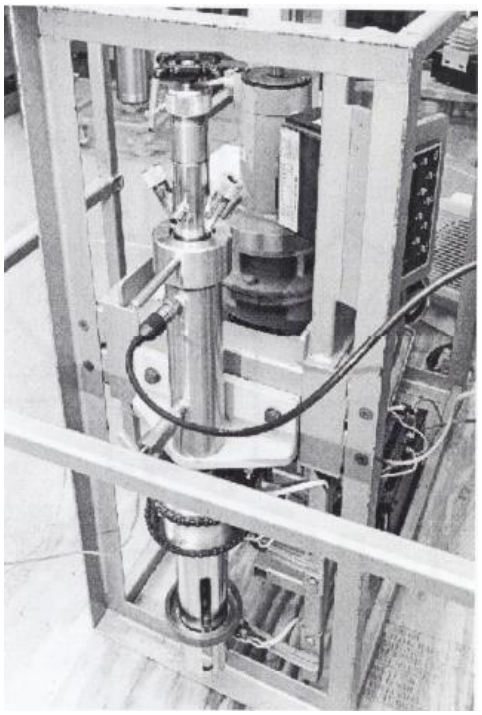

Figure 2: Experimental equipment inside the glass chamber.

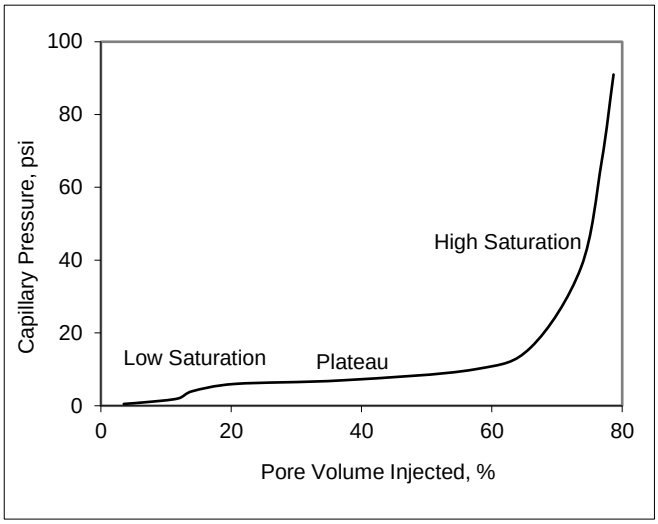

Figure 3: Core plug 3 capillary pressure versus mercury pore volume injected saturation.

The capillary pressure may increase to a level that has already been attained, shown as secondary in Figure 5, then it drops before increasing to a new level shown as tertiary in Figure 5. Mercury volume inserted from the primary capillary pressure drop commences until the tertiary pressure increase is reached equals the pore volume of interconnected pore bodies or system that has a threshold pressure less than or equals the pressure preceding the primary pressure drop. Compressibility tests are recommended for poor consolidated or compressible low permeability reservoir rocks where pores not yet filled by mercury might be compressed with increasing net overburden pressure as function of time. However, these tests are not relevant for the present high permeability and well-cemented Berea sandstone core plugs.

Figure 6 shows the basic principle of constant-rate mercury injection as the injected mercury pressure fluctuates with the porous media pore structure. Thus, detailed information on pore throats and pore bodies can be distinguished on the pressure fluctuations [17].

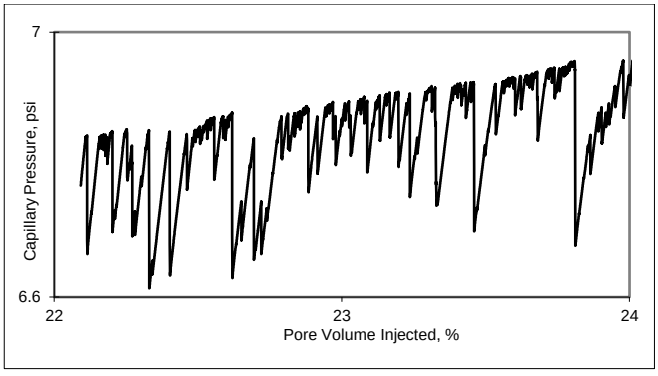

Figure 4: A magnified section shown the capillary pressure versus mercury volume injected divided by the ambient core plug pore volume.

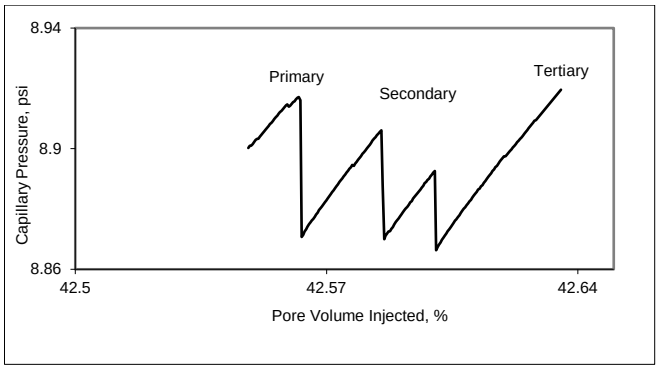

Figure 5: A magnified section from one of the experiments showing primary, secondary and tertiary pressure drops in an interconnected pore system.

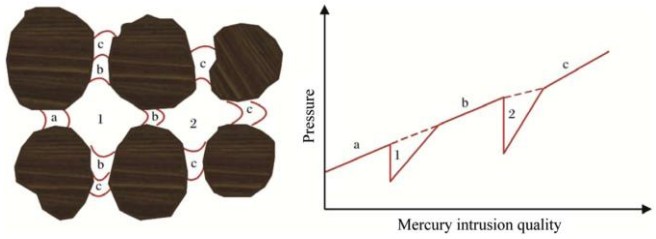

Figure 6: Schematic of the constant rate mercury injection process: a, b and c are throats, 1 and 2 are pores [17].

Laplace's equation is used to determine a pore throat effective entry radius:

$$r = \frac{2\,\sigma \cos\theta}{P_c} \qquad (1)$$

Where σ is the interfacial tension, θ is the contact angle, Pc is the capillary pressure obtained from the measured pressure-volume trace and r is the effective radius of the pore throat. For the calculation of the effective pore throat radius, the mercury/air contact angle equals 140° and the interfacial tension equals 480 mN/m invariant. These values were considered to be constant during the entire test because of the low rate of mercury injection applied during the experiments. As the capillary pressure increases to previously unattained levels, mercury meniscus advances into uninvaded pore throats. This analysis, therefore, resolves the rock pore space into pore throats and pore bodies, with each throat and pore is characterized by an entry volume and pressure.

Laplace's equation assumes straight capillary tubes, while in principle the rock pore network is model as a bundle of interconnected capillary tubes. Moreover, capillary hysteresis effects are not taken into account using this model. A program was developed to determine the number and volume of pore bodies. Volume of a pore body is determined by:

$$V_{pb} = \Delta P \left(\frac{dV}{dP}\right) \qquad (2)$$

Where $\left(\frac{dV}{dP}\right)$ is the rate constant determined from the pressure and time as shown in Figure 7. However, the above formula was modified to accommodate for the volumes of multiple smaller pores existing within an interconnected pore system. Volume of such system has previously been calculated by separating the pressure-volume fluctuations into compartments [18]. However, this method underestimates the invaded volume in a primary pore and overestimates the invaded volume in subsequent pores within the same system of interconnected pores [19]. Alternatively, multi-pore system was separated by extending the pressure-volume fluctuations vertically to the threshold pressure of the primary pressure drop assuming that the rate constant remains unchanged throughout the pores at a given pressure meaning $(dV/dP)_1 = (dV/dP)_2$ [19]. This might be true in an individual interconnected pore system, however, it was observed in the present study that the rate constant varies from one interconnected pore system to another. Therefore, average rate constant was considered for every individual interconnected pore system. For instance, the difference between rate constants, from one of the experiments, in two neighboring interconnected pore systems was 0.000134 cc/psi. The overall pore systems volume is determined by Equation 3 and as shown in Figure 8:

$$TV_{pb} = \left(\frac{dV}{dP}\right)_1 (\Delta P_{1r_1} + \Delta P_{2r_1} + \cdots) \left(\frac{dV}{dP}\right)_2 (\Delta P_{1r_2} + \cdots) + \left(\frac{dV}{dP}\right)_i (\Delta P_{1r_i} + \cdots) \qquad (3)$$

Where TV_{pb} is the total volume of the pore systems in the core plug, $(dV/dP)_1$ is the local rate constant in region number one, and $\Delta P_1 r_1$ is the pressure drop in region one, and so on.

Pore space morphology, rock fluid properties, local pore geometry and topology are factors that determine the distribution and volume of residual oil ganglia in the pore space or in other words pore and core scales heterogeneities [11, 20, 21]. In a drainage displacement, as mercury, being the non-wetting phase is injected into a rock, it preferentially occupies larger pores because of their low entry threshold pressure then it occupies smaller pores and throats. The large pores with low capillarity, therefore, would most likely trap the non-wetting phase in an imbibition displacement while the smaller throats are filled by the wetting phase.

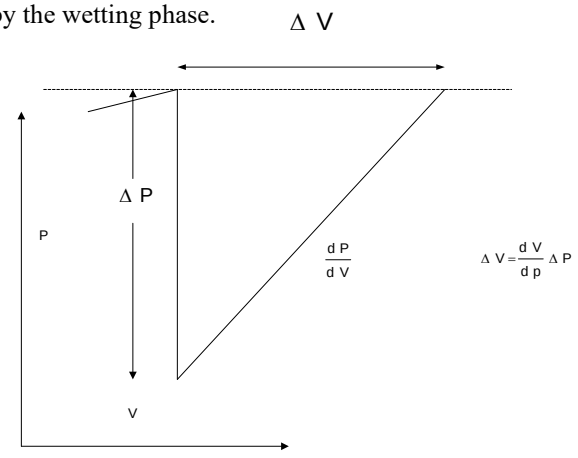

Figure 7: Rate constant determined from pressure and time.

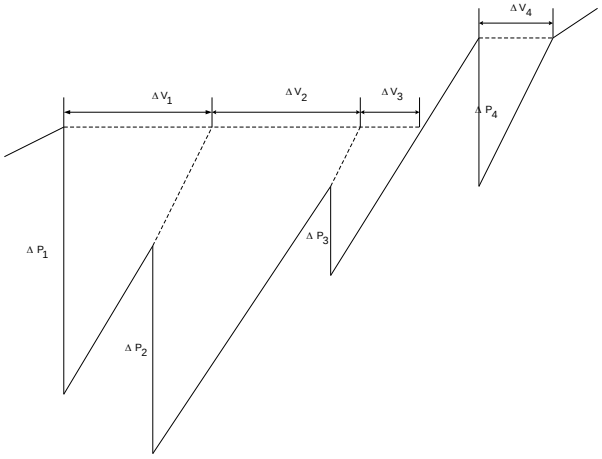

Figure 8: Volume determination of interconnected pore systems.

Because mercury is a strongly non-wetting phase, it can be assumed that snap-off disconnects the continuous filament of mercury and traps it in all pores during reduction of capillary pressure as the experiments is terminated [22].

The cumulative pore bodies' saturation provides good estimates of the residual mercury/air saturation assuming that all mercury is trapped in the pore bodies upon the experiment completion and pressure reduction [18]. Pressure was gradually decreased down to atmospheric pressure of 14.7 psi and sufficient time was given for capillary pressure-mercury saturation equilibrium. Thus, an imbibition cycle displacement takes place as the wetting phase (air) displaces the non-wetting phase (mercury). Therefore, cumulative volume of pores represents the final non-wetting phase saturation S_{nwr} that can be determined by:

$$\text{Snwr} = \sum_{i=1}^{N} \frac{V_{rs}}{V_p} \qquad (4)$$

N is the number of pores, V_{rs} is the volume of i pore and V_p is the core plug pore volume. Pore geometry affects the residual non-wetting phase saturation, which is the most important factor for the estimation or reservoir ultimate recovery and in any EOR operation. The value of residual non-wetting phase saturation by mercury entrapment might not be representative of the reservoir residual fluids saturation value. Mainly due to the fact that reservoir fluids wettability behavior is not properly reproduced during the experiment, as both mercury and air are by definition non-wetting phases.

4 Results and discussion

Figures 9 to 11 show the total rate-controlled mercury injection capillary pressure curve along with the individual pores and throats capillary pressure curves. In Figure 9, initial steep increase in capillary pressure due to entry effect where potential surface, irregular and truncated pores are initially filled. Then at mercury saturation of approximately 15.0 to 56.0%, overlapping takes place between total and pores capillary pressure curves. Mercury penetrates and fills large number of interconnected pore bodies as the capillary pressure increases to a threshold displacement pressure of around 2 psi, which renders a plateau in the total and pore capillary pressure curves followed by sharp increase in the capillary pressure with small increase in mercury saturation. There is slight increase in the capillary pressure in the plateau region with significant increase in mercury saturation. The total number of pores, occupied by mercury, for core plug 1 is 24138 occupying volume of 0.2234 cc. The throat capillary pressure curve, on the other hand, gradually increases as mercury is injected into the core plug. By the end of the experiment, the total mercury injection saturations of the pores and throats are 60.4 and 27.5%, respectively. Therefore, higher pores saturation than the throats saturation indicates that pores mostly control the overall displacement. The pores saturation of 60.4% also represents the residual non-wetting phase saturation or the final mercury entrapment saturation as detailed in section 3. Some throats might also trap mercury as the capillary pressure is reduced to atmospheric conditions, however, volume of mercury trapped in some throats is assumed to be negligible.

The pore throats of the well-sorted and highly permeable Berea sandstone rock might have similar sizes to the pore bodies. Moreover, as shown in Figure 4, the highly sensitive pressure transducer employed in the present study detects the smallest pressure fluctuations which indicates that distinguishing between pore throats and pore bodies is considerably arbitrary. Thus, similarly the distinction between pore throat capillary pressure and pore body capillary pressure curves is also considerably arbitrary. This indicates that pore throats still and also control the displacement and have an important portion of the Berea sandstone pore space. For this reason, the distinction between pore throats and pore bodies might be considered arbitrary.

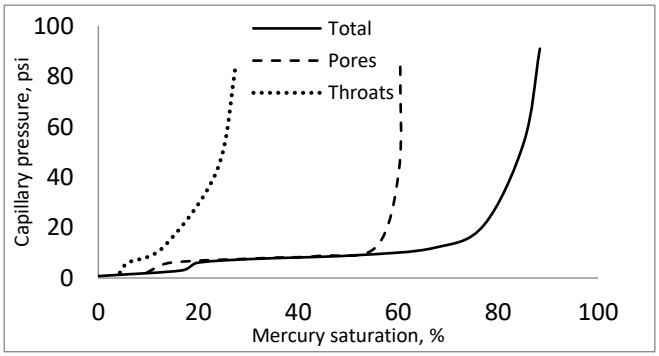

Figure 9: Core plug 1 mercury injection capillary pressure curves of the total, pores and throats.

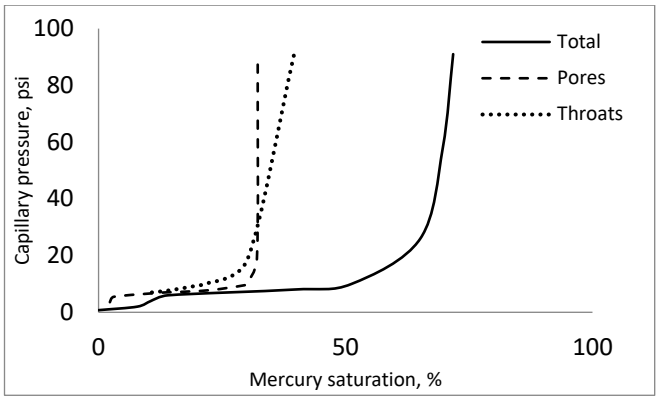

Figure 10: Core plug 2 mercury injection capillary pressure curves of the total, pores and throats.

Core plugs 2 and 3 shown in Figures 10 and 11, respectively have similar threshold displacement pressure of around 14 psi. The throat capillary pressure curves are higher than the pores capillary pressure curves. By the end of the experiment on core plug 2, the total mercury injection saturations of the pores and throats are 32.2 and 39.5%, respectively. The pores saturation of 32.2% also represents the residual mercury saturation.

By the end of the experiment on core plug 3, the total mercury injection saturations of the pores and throats are 32.3 and 46.3%, respectively. The pores saturation of 32.3% also represents the residual mercury saturation. The lower pores saturation than the throats saturation indicates that the throats mainly control the total mercury injection saturations of core plugs 2 and 3.

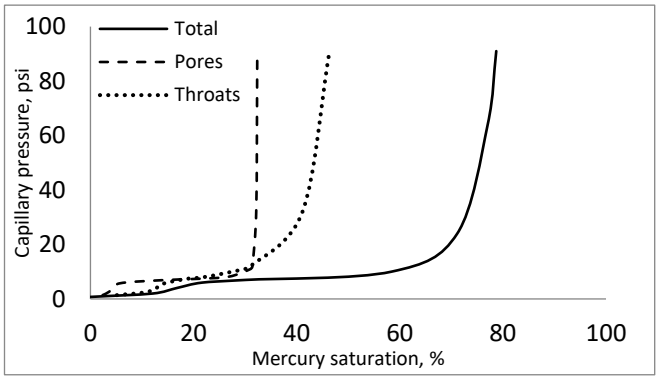

Figure 11: Core plug 3 mercury injection capillary pressure curves of the total, pores and throats.

The total number of pores, occupied by mercury, in core plug 2 is 21980 occupying volume of 0.2083 cc. The total number of pores, occupied by mercury, in core plug 3 is 21537 occupying volume of 0.2095 cc. The threshold displacement pressure of core plugs 2 and 3 is around 7 psi. As the threshold displacement pressure decreases, a lengthy overlap between the pore capillary pressure curve and the total capillary pressure curve exists while the overlap between the throat capillary pressure curve and the total capillary pressure curve is somewhat more evident as the threshold displacement pressure increases. Similar constant-rate mercury injection findings were reported for tight sandstone [3]. Shape of pore and throat capillary pressure curves variations as well as pore and throat occupancies between core plug 1 and core plugs 2 and 3, despite having the same lithology, textual properties and permeability, indicates that there is a cut-off limit to both spatial and local pore-throat correlations within the full diameter Berea sandstone core. Core plug 1 can be different or more heterogeneous at the pore network scale than core plugs 2 and 3. Thus, correlated heterogeneity at the pore scale may not extend to the sample size. Moreover, short-range correlations or local pore-throat correlations between pore bodies and the adjoining pore throats might not persist throughout the core plug. Therefore, large pore bodies do not necessarily adjoin large pore throats and small pore bodies do not necessarily adjoin small pore throats.

The volume and number distribution curves of the three core plugs are shown in Figure 12. Volume of pores distribution characteristics is similar for the three core plugs. It can be observed that the volume of pores ranges from 1 to more than 200 nL, however, peaking for the three core plugs at approximately 5 nL. In general, as porosity increases, the distribution of the volume of pores widens. This implies that even slightly tighter correlated sandstone may contain fewer pores and more wide and narrow throats.

Pore radius distribution curves of the three core plugs have similar characteristics as shown in Figure 13. Pore radii expand over a wide range from 0.0106 to 644 μm peaking at around 130 μm. Therefore, the pore radii of the Berea sandstone core plugs utilized contain nanopores, micropores and mesopores that are less than 1 μm, from 1 to 62.5 μm and from 62.5μm to 4 mm, respectively, according to Loucks et al. [23] pore classification. There might be no significant difference between the throat radius and pore radius distribution for large permeability core plugs [6].

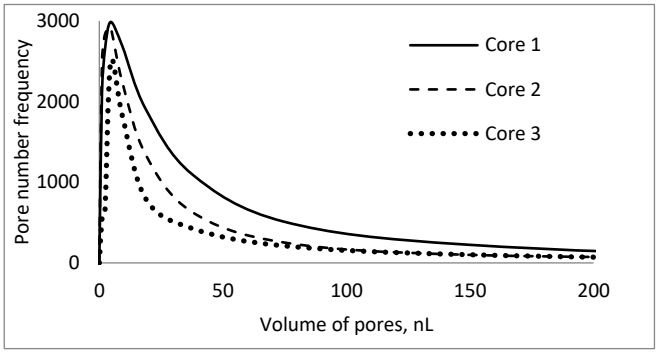

Figure 12: Volume and number distribution of the core plugs.

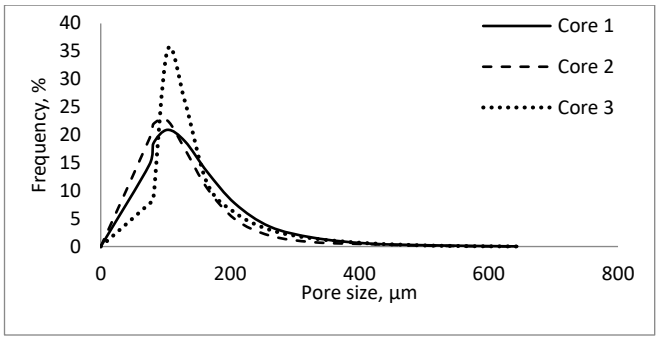

Figure 13: Core plugs pore size distributions.

Figure 3 shows a typical capillary pressure curve obtained from core plug 3 of the rate-controlled mercury injection experiments of the present work. The overall shape of the constant-rate mercury capillary pressure curve is similar to pressure-controlled capillary pressure curve. Equation 1 calculates the radius of a cylindrical capillary tube; however, Berea sandstone and all reservoir rocks have complex pore throats and bodies geometry and structural configurations that are very complex in geometry. Therefore, the calculated values of pore throats represent the effective radii of the pore throats that might not equal their actual dimensions. Figure 3 shows a flat and broad plateau indicating well-sorted correlated Berea sandstone dominated by throats of similar sizes. Previous studies on pore-throat correlated networks revealed that steepness of drainage capillary pressure curves decrease as correlations increase [24, 25].

The maximum pressure achieved during the experiments of the present work is around 91 psi, which was sufficient for mercury to penetrate up to around 88.0% of the pore space. Some of the previous rate-controlled mercury injection experiments underwent maximum mercury injection pressure of 899 psi especially when tight rocks were used [3]. Overall, the significant pressure increase towards the end of the experiments with small increase in mercury saturation indicates that the injected mercury only fills some unfilled small pores and throats as shown in Figure 14. Capillary pressure fluctuations in these pores and throats are very small, even when plotted on magnified scale as in Figure 14, because the relative injection rate relative to the pore volume is very high. As the relative mercury rate becomes high, the resultant capillary pressure curve is similar to that obtained by constant-pressure mercury porosimetry where pores and throats filling times are extremely short for the pressure transducer to detect or resolve.

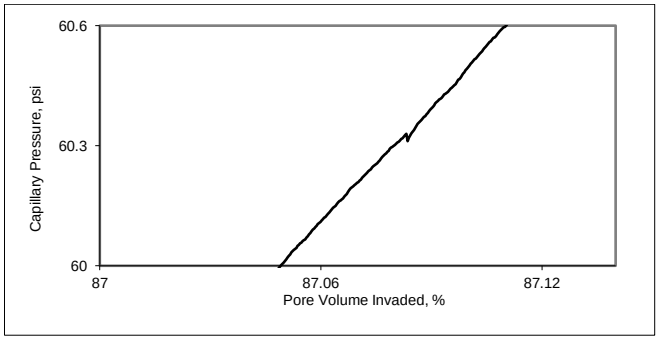

Figure 14: Capillary pressure fluctuations towards the end of the experiment.

Calibrations of the interpretations of the present study with petrographic observations, such as optical and electron microscopy, of the pore types, pore texture, and pore throats was not performed mainly due to health and safety reasons. However, to address the uncertainties concerning the calibration of the interpretation, some previously published data on pore geometry from petrographic observations maybe used. Figure 15 shows a back-scattered electron (BSE) image of petrographic thin section of Berea sandstone [26]; the pore space is black, quartz is medium grey, feldspar is light grey, and clays are dark grey.

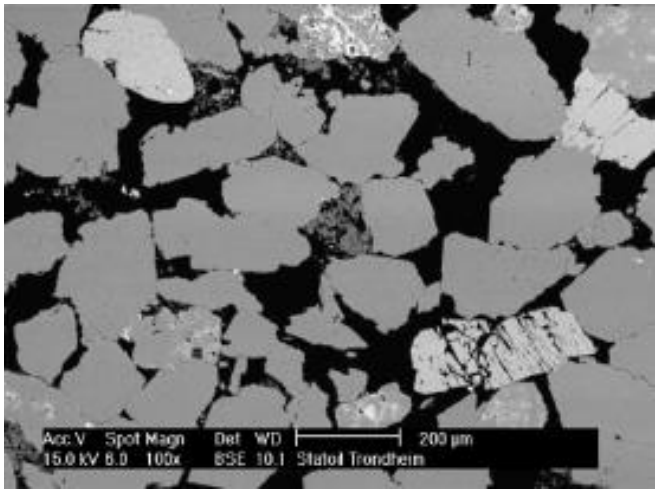

Figure 15: Back-scattered electron image of a thin section of Berea sandstone [26].

Figure 16 shows a scanning electron microscope image of Berea sandstone; clays was found to preferentially coat the quartz grains that resulted in no correlation between the modal mineral composition of the rock and the fraction of surface area made up by the mineral [27].

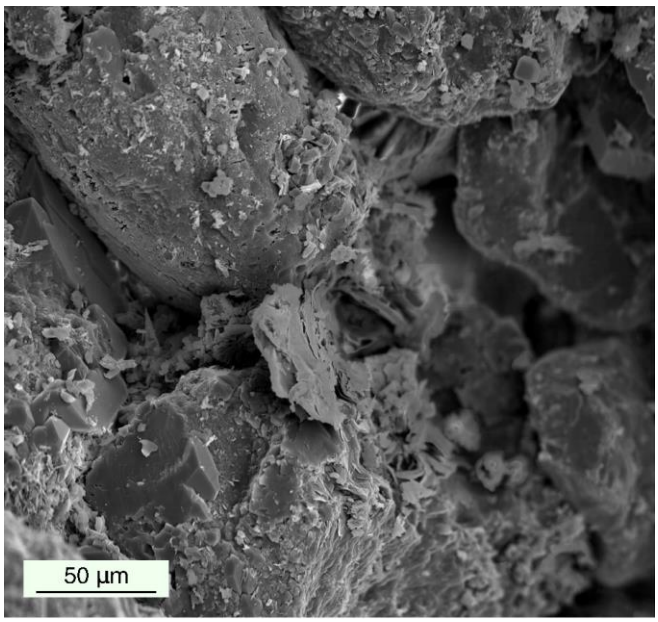

Figure 16: Scanning electron microscope image of Berea sandstone [27].

Figure 17 shows a microtomographic image of Berea sandstone slice [28]. Berea sandstone was characterized by an increase in porosity, resulting in a higher coordination number and characterized by a dense network of numerous smaller throats and pores of radii ~1.3 and ~2.7 μm, respectively.

Figures 15 and 17 show that Berea sandstone, and all porous rocks, is composed of grains, pore bodies and throats. The pore bodies represent the voids or spaces between the rock mineral grains, and the throats are narrow tubes or channels in the rock that connect all different types of pores. The rate-controlled results of the present study reveal that the pore size ranges from 0.0106 to 644 μm. Figures 15 to 17 of the petrographic microscopic observations show that pore sizes fall within the experimentally determined range. Therefore, rate-controlled mercury experiments can effectively characterize a wide range of Berea sandstone pores. However, the accuracy of these findings can only be ensured when the petrographic microscopic thin sections are performed for the same core plugs subjected to the rate-controlled mercury injection experiments.

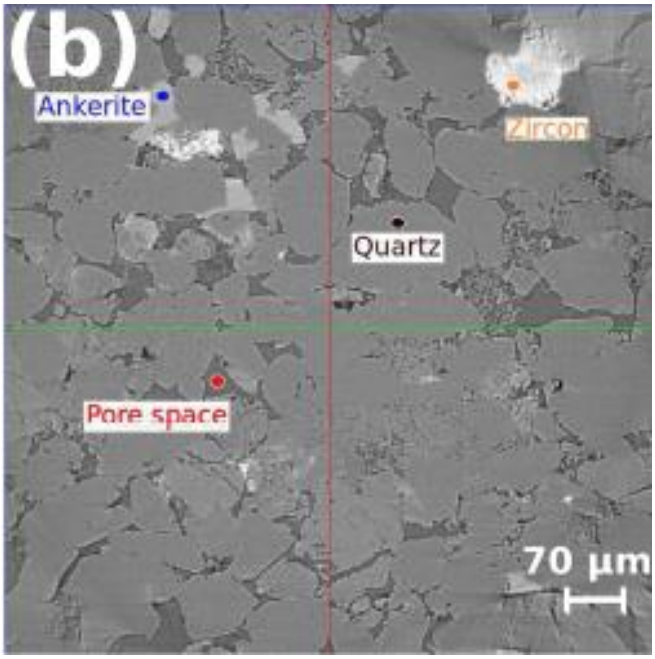

Figure 17: Microtomographic image of Berea sandstone slice [28].

5 Conclusions

Rate-controlled mercury porosimetry equipment was constructed and used to characterize Berea sandstone rock into pore bodies and pore throats. Three capillary pressure curves were obtained; one describes the larger pore spaces or pore bodies of the rock core plug, another describes the smaller pores or pore throats that connect the larger pores, and a final curve which corresponds to the overall capillary pressure curve, similar to that obtained from the conventional pressure-controlled mercury injection. The Berea sandstone used had good physical properties with a porosity ranged from 28.2 to 30.7% and gas permeability of 1.31 D. Information on the statistical nature of the pore structure and heterogeneity were obtained as pressure fluctuations with time revealed menisci locations of pore bodies and throats.

Pore size distributions based on volume-accessed pores and pore radii were obtained from the pressure versus saturation relationship. The radii of the pores ranged from 0.0106 to 644 μm indicating that pore radius classification included nanopores, micropores and mesopores; however, the majority of pore radii were mesopores. Results matched previously published petrographic observations data on Berea sandstone.

One of the constraints of rate-controlled mercury injection technique is that the experimental pressure is generally low; therefore, maybe limited nanopores' radii threshold entry pressure can be exceeded. Although pore bodies control the porosity, throats also constitute an appreciable portion of the pore space volume. Varying pore and throat capillary pressure curves obtained for the Berea sandstone core plugs indicate complex geometry of the throats and pores systems. Furthermore, the shapes of the total capillary curves indicate that the core plugs' local pore throats and spatial correlations persist and pore distribution can still be heterogeneous within the same core plug. It is important to mention that despite the valuable pore space morphology characteristics and hydrocarbon saturation information that the rate-controlled mercury injection technique provides, it is also financially costly, very slow to conduct and labor intensive compared to the routine conventional pressure-controlled mercury injection techniques. The experimental procedure is also extremely time consuming and data processing is complex.

References

1. H.H. Yuan and B.F. Swanson. SPE Form. Eval. **4**, 17-24 (1989).
2. H. Gao, T. Li and L. Yang. J Petrol Explor Prod Technol. **6**, 309–318 (2016). https://doi.org/10.1007/s13202-015-0186-6
3. W. Zhang, Z. Shi and Y.Tian. Energy Explor. Exploit. **38**(6), 2389-2412 (2020). doi: 10.1177/0144598720920729.
4. J. Smith and I. Chatzis. Canada: N. p., (2004).
5. Y. Zhang, Z. Bao, F. Yang, S. Mao, J. Song, L. Jiang. Geofluids. 2018, ID 3403026 (2018). https://doi.org/10.1155/2018/3403026
6. C. Zhang, Y. Cheng and C. Zhang. J. of Geophys. Eng. **14**, 132-142(2017).
7. Y. Wang, Y. Gao and Z. Fang. Petrol. Explor. Develop. **48**(2): 308-322(2021).
8. B.F. Swanson. J. Pet. Technol. 10-18(1979).
9. N.C. Wardlaw, N.C. Li and D. Forbes. Transp Porous Media. 2, 597-614(1987).
10. A. Makse, H. Hernan, P.S. Ivanov et al. Physica A. **233**, 587-605(1996).
11. C.D. Tsakiroglou and A.C. Payatakes. J. Colloid Interface Sci. **2**, 479-494(1991).
12. J. Liu, S. Song, X. Cao, Q. Meng, H. Pu, Y. Wang, J Liu. J. Rock Mech. Geotech. Eng. 12(2), 403-413(2020).
13. Y. Yao and D. Liu. Fuel. **95**, 152-158(2012).

14. A. J. Adams. Doctoral dissertation, Texas A&M University. Texas A&M University, (2005).
15. W.M. Mahmud. Pet. Sci. Eng. **2**(1):23-29(2017).
16. W.B. Haines. J. Agri. Sci. 20, 97-116 (1930).
17. H.-Y. Zhu, L.-Z. An and C.-Y. Jiao. Natural Gas Geoscience. **26**(7):1316-1322 (2015).
18. H.H. Yuan. SPE 19617 (1989).
19. G. Mason. SPE Form. Eval. (1991).
20. N.R. Morrow. J. Can. Pet. Technol. 35-46(1979).
21. H.K. Christenson, J.N. Israelachvili and R.M. Pashley. SPE Reserv. Eng. 155-165(1987).
22. W.M. Mahmud and V.H. Nguyen. Trans. In Por. Media. **64**, 279-300(2006).
23. R.G. Loucks, R.M. Reed, S.C. Ruppel, et al. AAPG Bulletin **96**(6): 1071–1098 (2012).
24. Y. Li, W.G. Laidlaw and N.C. Wardlaw. Adv. Colloid Interface Sci. 26,1-86(1986).
25. M.A. Ioannidis and I. Chatzis. Water Resour. Res. **29**, 1777-1785(1993).
26. P-E. Øren and S. Bakke. J PETROL SCI ENG. **39**(3-4), 177-199 (2003).
27. P. Lai, K. Moulton and S. Krevor. Chem. Geol. **411**, 260-273 (2015).
28. T. Paul-Ross, A-Z. Aizhan, H-M. Saswata. Front. Earth Sci. **6** (2018).